RSC Advances

PAPER

View Article Online
View Journal | View Issue

Cite this: *RSC Adv.*, 2026, **16**, 25439

Practical synthesis and photophysical characterization of full-color circularly polarized luminescent 4,7-diaryl-5,6-(*R*/*S*)-BINOL-*O*-[2,1,3] benzothiadiazoles

Trang T. T. Pham,†[a] Phuong T. H. Chu,†[a] Bach L. D. Hoang,[a] Chau M. Vo,[a] Duan V. Le,[a] Hien Nguyen,[c] Thanh-Tuân Bui,[b] Gioi V. Nguyen,[a] Nikita Salov,[d] Gregory Pieters[d] and Tung T. Dang*[a]

Received 7th December 2025
Accepted 30th March 2026

DOI: 10.1039/d5ra09454b

rsc.li/rsc-advances

4,7-Dibromo-5,6-(*R*/*S*)-BINOL-*O*-2,1,3-benzothiadiazole (**10**) was synthesized quantitatively by an S_NAr reaction of *R*/*S*-BINOL and 5,6-difluoro-2,1,3-benzothiadiazole in gram scale and is emerging as an important building block for the construction of circularly polarized luminescent organic materials. The 4,7-diarylated-5,6-(*R*/*S*)-BINOL-*O*-2,1,3-benzothiadiazoles have been successfully synthesized *via* Suzuki cross-coupling reaction with various aryl boronic acids. This synthetic approach is a practical and useful tool to tune circularly polarized luminescent properties.

Introduction

BINOL, or 1,1′-bi-2-naphthol, is a well-known axially chiral molecule that was initially synthesized in 1926.[1] Due to its stable chiral configuration and versatile functionalities, BINOL and its derivatives are widely recognized as essential chiral scaffolds in the field of asymmetric synthesis and materials science.[2–6] Its unique biaryl structure and excellent chirality transfer properties make it a valuable ligand in various catalytic reactions, including asymmetric oxidation, reduction, and C–C bond forming reactions, as highlighted in the advances of its synthesis methods.[2–7] Moreover, BINOLs can coordinate with various metal centers such as aluminum and copper, thereby expanding their utility in asymmetric catalysis, offering diverse synthetic possibilities.[8,9] BINOL's use in mechanically interlocked molecules (MIMs) facilitates chirality transfer, asymmetric catalysis, and stereoselective chemo-sensing, with future advancements possible through the inclusion of additional stereogenic elements or mechanical chirality.[10] The incorporation of BINOL into metal–organic frameworks (MOFs) has led to the creation of fluorescent sensors with impressive enantioselectivity ratios, crucial for pharmaceutical applications, which can effectively discriminate between enantiomers and be vital for drug safety and efficacy.[11] BINOL derivatives, especially BINOL-based polymers, exhibit unique circularly polarized luminescence (CPL) characteristics, a phenomenon where light is emitted with a specific handedness of circular polarization, particularly when integrated into solid-state materials or solutions, enhancing their luminescent properties through chiral perturbation mechanisms.[6,12] de la Moya and his co-workers introduced a structural design for CPL using inherently achiral BODIPY chromophores paired with a BINOL unit, highlighting their potential for developing simple, highly functional CPL dyes with tunable properties for diverse photonic and biomolecular applications.[13] Furthermore, the attachment of an axially chiral binaphthyl group to the helical carbazole-based BODIPY structures could enhance the chiroptical properties of the analogs.[14] Besides being able to integrate with metals in asymmetric synthesis, BINOL can also be bound to Pt to form two chiral complexes, exhibiting both aggregation-induced phosphorescence and circularly polarized luminescence.[4]

In the context of optoelectronic devices, BINOL derivatives (Fig. 1) have been widely explored as CPL emitters for circularly polarized organic light-emitting diodes (CP-OLEDs), offering unique advantages such as improved energy efficiency, polarization control, and enhanced display quality. The BINOL unit, with its strong conjugation effects and excellent ability to induce chirality in polymer matrices and small organic molecules, along with circularly polarized emission through chiral perturbation, facilitating its integration into thermally activated delayed fluorescence (TADF) materials, has led to notable advancements in organic light-emitting diode (OLED) technology.[15–17] The ability to functionalize BINOL through modern synthetic methods and techniques provides a powerful

[a]*Hanoi University of Science and Technology, 1 DaiCoViet, Hanoi, Vietnam. E-mail: tung.dangthanh@hust.edu.vn*

[b]*CY Cergy Paris Université, LPPI, F-95000 Cergy, France*

[c]*Department of Chemistry, Hanoi University of Educational University, Vietnam*

[d]*Université Paris-Saclay, CEA, INRAE, Département Médicaments et Technologies pour la Santé (DMTS), SCBM, Gif-sur-Yvettes F-91191, France*

† These authors contributed equally.

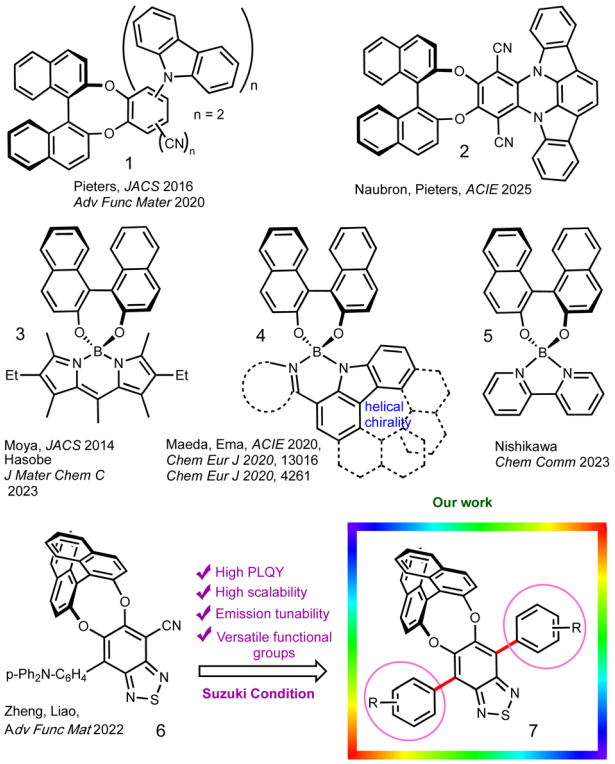

Fig. 1 Circularly polarized luminescent organic and organometallic materials based on BINOL atropisomer.

route to tune its optical and electronic properties, thereby expanding its application potential.[18]

The design of BINOL with donor–acceptor (D–A) structures represents a highly promising strategy for developing advanced materials for CP-OLED applications. For example, Pieters and co-workers successfully developed BINOL-based TADF materials in a chiral A–D architecture, achieving high quantum yields and external quantum efficiency, marking a significant advancement in CP-OLED research in which benzenedicarbonitrile acts as an acceptor unit of the TADF materials, and carbazole and indolocarbazole are the donor moieties.[15,19,20] Recently, incorporating electron-deficient heterocyclic systems into the BINOL framework further elevated its utility in CPL-active materials. Among them, benzothiadiazole (BTD) is a well-known acceptor unit with strong electron-withdrawing properties, high thermal stability, and photostability, making it a versatile fluorophore building block widely used in many applications, including luminescent materials, organic light-emitting diodes, organic solar cells, organic field-effect transistors, biosensors, bio-imaging, and other applications.[21–29] Recently, Zheng and co-workers introduced a fluorescent material based on BTD and chiral binaphthol, enabling CPL and hybridized local and charge transfer (HLCT) properties, achieving high external quantum efficiency (EQE) and exciton utilization in CP-OLEDs, with further efficiency improvements through sensitization by a TADF material. However, the number of compounds synthesized in previous studies has been limited, thereby restricting the exploration and investigation of their optoelectronic properties, the structure–property relationships, as well as their potential applications.[30]

Numerous studies have proposed synthesis methods and highlighted the functionalization of BINOL derivatives as well as benzothiadiazole derivatives. Palladium-catalyzed coupling reactions are considered one of the most efficient and versatile methods. Our research focuses on the practical synthesis of 4,7-dibromo-5,6-(*R*/*S*)-BINOL-*O*-2,1,3-benzothiadiazole with 18 different boronic acids *via* Suzuki cross-coupling reactions to generate a library of CPL-active derivatives. By combining the chiral properties of BINOL with the electronic characteristics of benzothiadiazole, this work provides a robust platform for the design of next-generation CPL materials with tailored properties for advanced optoelectronic applications.

Results and discussion

Firstly, our synthetic strategy began with a nucleophilic aromatic substitution reaction between commercially available 4,7-dibromo-5,6-difluoro-2,1,3-benzothiadiazole (**9**) and optically pure (*R*/*S*)-BINOL (**8**), affording intermediate (**10**) in a 97% yield on gram scale. This transformation proceeded efficiently under mild conditions, showcasing the reactivity of the difluorinated benzothiadiazole core towards BINOL-based nucleophiles. Subsequent Suzuki–Miyaura cross-coupling reactions were performed between the intermediate (**10**) and a variety of aryl boronic acids. This step yielded a series of novel 4,7-diaryl-substituted 5,6-(*R*/*S*)-BINOL-benzothiadiazole derivatives (**7a–7s**) in moderate to good yields (69–94%). The synthetic details, including reaction conditions, yields, and purified products, are summarized in Scheme 1.

The Suzuki coupling reactions proceeded efficiently across a wide range of aryl boronic acids, with reaction outcomes strongly influenced by the nature of the substituent. Compounds bearing simple phenyl and alkyl-substituted aryl groups (**7a–7d** and **7q**) exhibited the highest yields with clean profiles and easy purification, with **7b** reaching 94%. Compounds with electron-donating groups such as methoxy and dimethylamino (**7f–7h** and **7s**) were also prepared in high yields (86–75%), consistent with the favorable electronic influence of donors on the coupling process. In contrast, the formyl-substituted derivatives (**7j** and **7k**) were obtained with slightly lower yields (72% and 76%, respectively), likely due to the electron-withdrawing nature of the aldehyde group, which reduces the nucleophilicity of boronic acid, and the potential sensitivity under coupling conditions; these products were slightly more challenging to purify but showed clearly distinguishable aldehyde signals in ^{1}H NMR spectra. Heteroaryl boronic acids (**7l–7n**) offered consistently good yields (87–93%), demonstrating their compatibility with the reaction system and clean separation.

All final compounds were fully characterized by ^{1}H and ^{13}C NMR spectroscopy, confirming the expected structures (Fig. 2, S3 and S4). Of particular interest are compounds **7d** and **7l**, which showed significantly more complex NMR spectra due to the presence of multiple isomers. Owing to steric hindrance and restricted rotation around the aryl–aryl single bonds formed

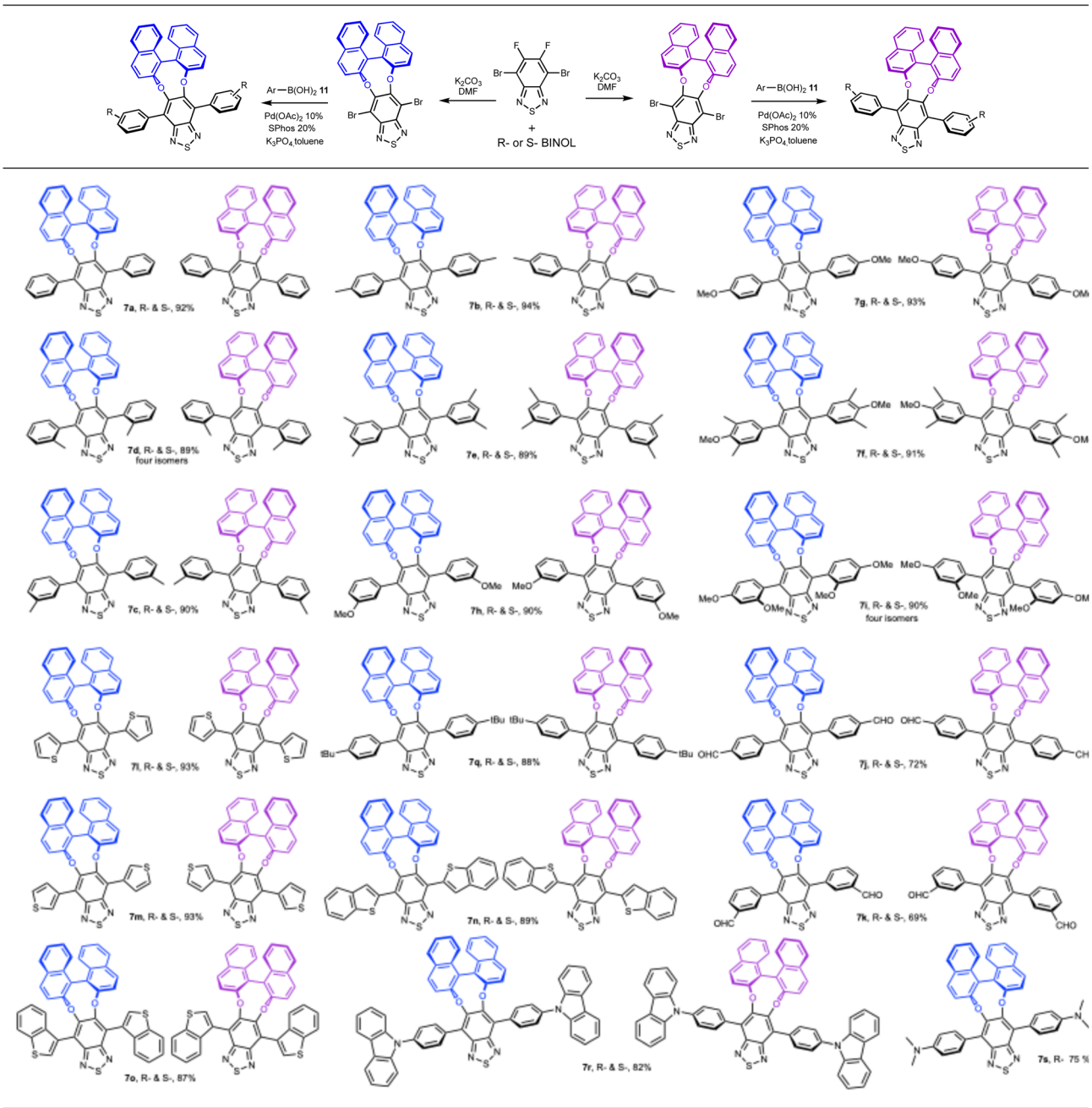

Scheme 1 Scope of Suzuki reaction of 4,7-dibromo-5,6-(*R*/*S*)-BINOL-benzothiadiazole. Reaction condition: (i) **8** (1 equiv.), **9** (1 equiv.), K_2CO_3 (3 equiv.), and DMF (3 mL) at 80 °C. (ii) **11** (4 equiv.), $Pd(OAc)_2$ (10 mol%), SPhos (20 mol%), K_3PO_4 (4 equiv.), and toluene (3 mL) at 100 °C.

between the chiral BINOL-*O*-benzothiadiazole core and the substituted aryl groups, these compounds exhibit four distinct atropisomers in solution. This results in the splitting of NMR signals into four separate sets, corresponding to each isomer. In the ^{1}H NMR spectra of **7d** and **7l** (Fig. S25 and S41), this phenomenon is clearly visible as multiple sets of signals, often appearing as four separate peaks or peak clusters for protons in symmetric environments of the rigid core. Specifically, this phenomenon can be observed in the aliphatic region, each signal corresponding to one isomer, while the signal of protons in the aromatic region easily overlaps with other signals, making it challenging to separately identify the signals of each isomer. In addition, the different peak heights of each isomer could come from the existing ratio in the mixture. Similarly, the ^{13}C NMR spectra exhibit fourfold splitting of several carbon signals, further supporting the presence of multiple stable conformers (Fig. S26 and S42).

Interestingly, under the same Suzuki cross-coupling conditions employed for all substrates, the reaction between (*R*/*S*)-**10** and 4-(*N*,*N*-dimethylamino)phenylboronic acid exclusively afforded the mono-arylated product (**7s**) rather than the expected bis-arylated derivative. Thin-layer chromatography (TLC)

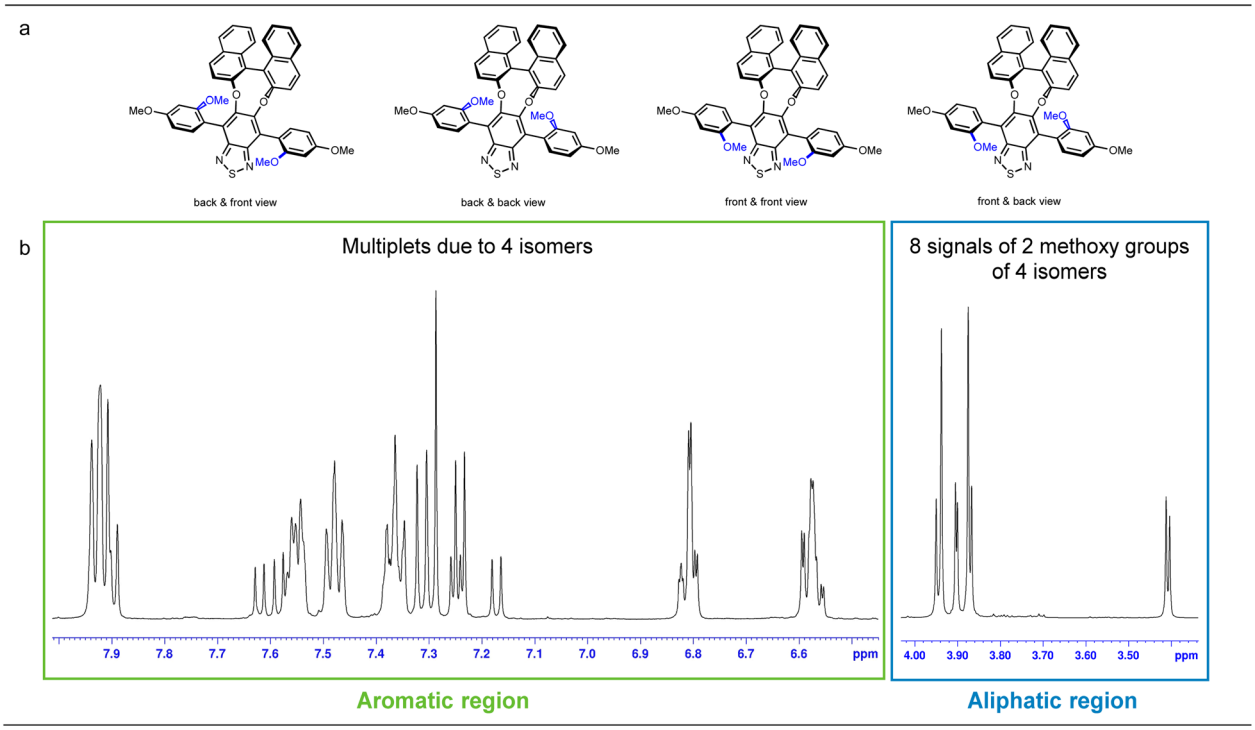

Fig. 2 (a) Structure of 4 isomers of **7i** and (b) ^{1}H NMR spectra of these 4 isomers.

monitoring indicated a single product spot, and subsequent purification yielded **7s** as the sole product, with a moderate isolated yield of approximately 65%. The structure was unambiguously confirmed by ^{1}H and ^{13}C NMR spectroscopy (Fig. S50 and S51) and mass spectrometry, with NMR spectra showing characteristic signals consistent with mono-arylation. This selectivity is likely attributed to the strong electron-donating nature of the *N*,*N*-dimethylamino group, which may significantly reduce the reactivity of the intermediate brominated species toward a second cross-coupling event, possibly by electron density redistribution or steric hindrance.

The photophysical behavior of compounds **7a–7s** was systematically investigated in dichloromethane (DCM) solution, revealing their structure–property relationships. Representative photophysical data are summarized in Fig. 3a, b, S6, S7, and Table 1. The absorption spectra, dominated by π–π* and ICT transitions, ranged from 317 to 448 nm, depending on the aryl substituent. Unsubstituted phenyl and alkyl-substituted derivatives (**7a–7d** and **7q**) exhibited absorptions near 325–328 nm, while donor-containing compounds (**7f–7h**, **7r** and **7s**) showed significant bathochromic shifts up to 440 nm, attributed to enhanced intramolecular charge transfer (ICT). In contrast, formyl-substituted derivatives (**7j** and **7k**) presented blue-shifted absorption around 317–323 nm, reflecting their electron-deficient nature, which weakens the D–A interaction.

The emission spectra spanned a wide range (418–695 nm), tunable through electronic modulation. Simple alkyl-substituted derivatives like **7c** and **7d** emitted around 454–470 nm, while more electron-rich systems such as **7g**, **7h**, and **7s** displayed emission maxima significantly red-shifted to 491 nm, 518 nm, and 695 nm, respectively. Notably, **7s** showed the most red-shifted emission of all compounds, consistent with the strong donor ability of the *N*,*N*-dimethyl group, enhancing conjugation. Similarly, **7r** displayed an emission maximum at 528 nm, illustrating the contribution of extended π-conjugation from the rigid donor moiety. Particularly interesting are the heteroaryl derivatives (**7l–7n**), which showed red-shifted emission relative to their phenyl counterparts, suggesting strong conjugation between the heterocyclic π-system and the benzothiadiazole core. This trend follows the increased aromatic character and conjugation length of the heteroaryl group. These findings underscore the critical role of heteroatoms and fused-ring systems in fine-tuning the optical properties through modulation of the electronic delocalization.

The chiroptical properties of the enantiopure (*R*)- and (*S*)-**7b**, **7g**, **7l**, **7n**, and **7q** were evaluated using electronic circular dichroism (ECD) spectroscopy (Fig. 3) in chloroform as well as circularly polarized luminescence (CPL) spectroscopy in DCM solutions (Fig. 3) at 295 K. As illustrated in Fig. 3c, each enantiomeric pair exhibited a perfect mirror-image relationship, demonstrating that chirality was fully preserved throughout the reaction sequence. Relatively intense ECD signals were observed between 300 and 400 nm, corresponding to π–π* transitions of the conjugated benzothiadiazole framework. Compound **7g** showed the strongest positive ECD signal around 320 nm ($\Delta\varepsilon \approx +77$ M^{-1} cm^{-1}), indicating enhanced chiral electronic transitions from the electron-donating group. Heteroaryl derivatives **7l** and **7n** displayed broader, red-shifted responses with slightly lower intensities ($\Delta\varepsilon \approx +58$ and $+35$ M^{-1} cm^{-1}). Meanwhile, **7b** and **7q** maintained sharp

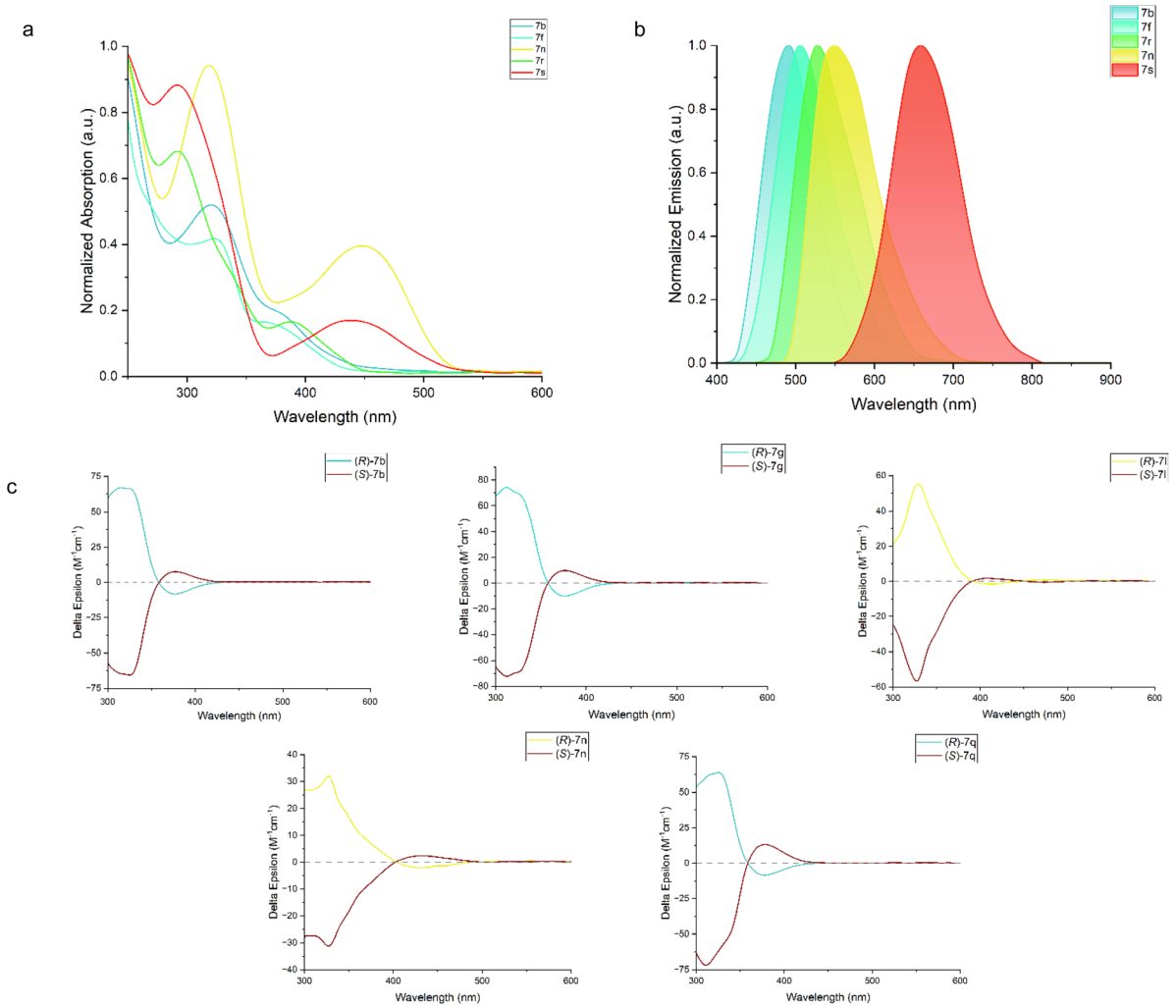

Fig. 3 (a) Normalized UV-visible electronic absorption spectra and (b) normalized photoluminescence spectra (filled areas) of **7b**, **7f**, **7n**, and **7r**. (c) Electronic circular dichroism (ECD) spectra of (*R*)- and (*S*)-enantiomers of **7b**, **7g**, **7l**, **7n** and **7q** measured at 295 K. Transient decay profile of compound **7l** in the solid state. All experimental spectra were recorded in DCM (10^{-5} M). All detailed properties are shown in Table 1.

Table 1 Photophysical and theoretical calculation data of **7a–7s** in DCM

Compound	λ_{abs} (nm)	λ_{em} (nm)	Stokes shift (nm)	HOMO (eV)	LUMO (eV)	ΔE (eV)
7a	328	475.2	147.2	−5.86	−2.56	3.31
7b	327	490.4	163.4	−5.87	−2.48	3.38
7c	325	478.4	153.4	−5.98	−2.54	3.44
7d	326	454.4	128.4	−6.04	−2.53	3.51
7e	324	484.8	160.8	−5.91	−2.46	3.45
7f	326	506.4	180.4	−5.79	−2.46	3.33
7g	327	491.2	164.2	−5.59	−2.44	3.15
7h	324	481.6	157.6	−5.89	−2.58	3.32
7i	319	518.3	199.3	−5.59	−2.29	3.29
7j	317	—	—	−6.24	−3.04	3.21
7k	322	—	—	−6.21	−2.77	3.43
7l	435	544.7	109.7	−5.54	−2.73	2.81
7m	318	510.4	192.4	−5.81	−2.64	3.18
7n	448	550.2	102.2	−5.57	−2.86	2.71
7o	324	506.4	182.4	−5.86	−2.64	3.22
7q	326	490.4	164.4	−5.87	−2.48	3.38
7r	388	527.9	139.9	−5.58	−2.78	2.80
7s	438	654.7	216.7			

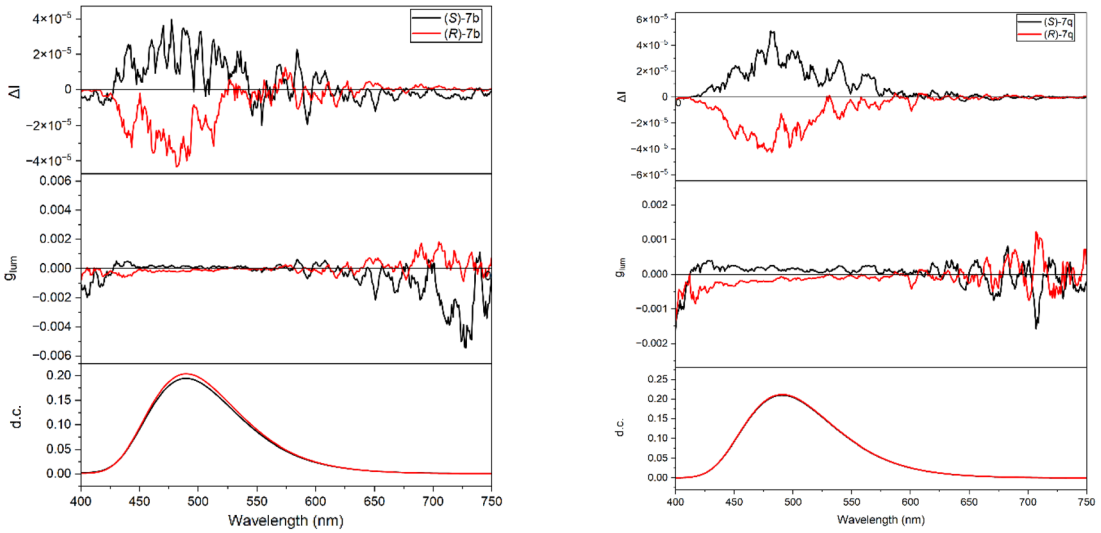

Fig. 4 CPL (upper curves), g_{lum} (middle curves) and total luminescence (lower curves) spectra of (*R*) (red curve) and (*S*) (black curve) of **7b** and **7q** in DCM (10^{-4} M) at 295 K, excitation at 350 nm.

signals, showing that alkyl groups exert minimal influence on ECD intensity. Concerning the CPL measurements (Fig. 4), nearly perfect mirror-image CPL emission profiles were observed for each enantiomeric pair of **7b** and **7q**. The corresponding g_{lum} values at the emission maxima reached 1.7×10^{-4} for **7b** and $\pm 2.4 \times 10^{-4}$ for **7q** in DCM solution.

To gain more insight into the electronic properties and geometrical structures and to correlate the frontier orbital energies of the obtained compounds, theoretical calculations were performed using density functional theory (DFT) with the B3LYP/6-31g(d,p) method. As shown in Fig. 5, Table 1, and Fig. S3–S5 in the SI, the calculated HOMO–LUMO gaps (ΔE) across the series range from 3.44 eV (**7c**) to 2.71 eV (**7n** and **7s**), correlating well with the experimentally observed emission trends: compounds with lower energy band gap values generally exhibit longer-wavelength emission. We can easily observe that the HOMOs in most cases are primarily distributed over the π-conjugated system of the BTD core and the aryl substituent, while the LUMOs remain primarily on the electron-deficient BTD moiety. Notably, the HOMO–LUMO gaps of **7bs**, are calculated as they are moderately separated (ΔE = 3.38 eV), corresponding to its relatively blue emission at 490.4 nm, while

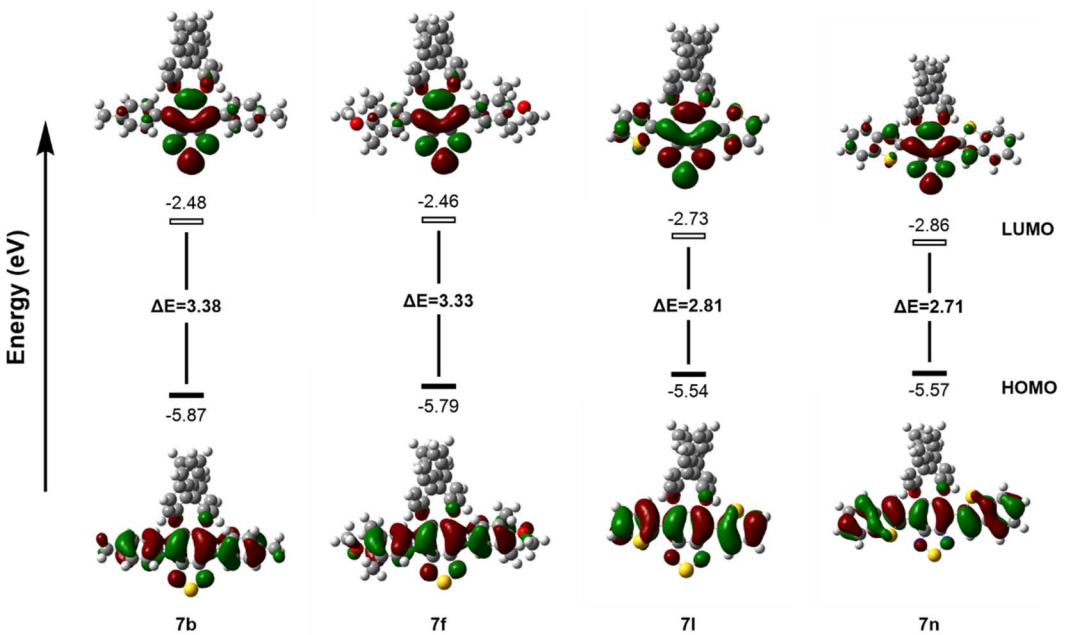

Fig. 5 Distribution of HOMO and LUMO of compound **7b**, **7f**, **7l** and **7n**.

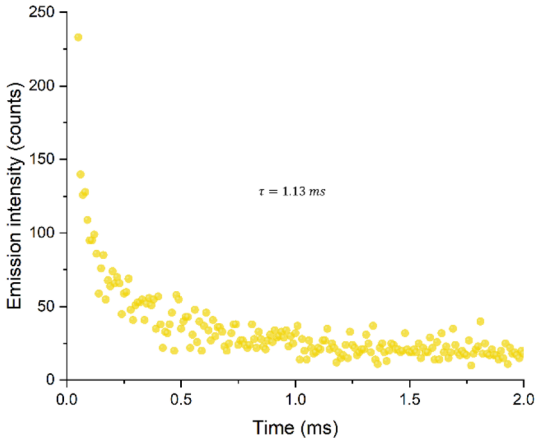

Fig. 6 PL decay curve of compound **7m** in solid state.

the introduction of an electron-donating methoxy group slightly raises the HOMO level (−5.79 eV) of **7f**, yielding a quite lower ΔE of 3.33 eV, showing that the HOMO–LUMO distributions begin to show increased orbital overlap between donor and acceptor. Moving to heterocycles, **7l** and especially **7n** demonstrate significantly narrower bandgaps (2.81 eV and 2.71 eV, respectively), driven by stabilized LUMOs and elevated HOMOs due to their extended π-systems. Their HOMO–LUMO distributions display pronounced charge delocalization across the heteroaryl substituents and the BTD core, enabling more effective donor–acceptor conjugation. This enhanced ICT character results in strong bathochromic emission shifts.

Notably, the time-resolved photoluminescence measurements of compound **7m** in the solid state revealed a relatively long emission lifetime of τ = 1.13 ms (Fig. 6). This lifetime, which is orders of magnitude longer than typical fluorescence (nanosecond scale), strongly indicates the involvement of triplet excited states. Such a millisecond-scale decay is possibly consistent with phosphorescent emission,[30,31] facilitated by efficient intersystem crossing (ISC) between singlet and triplet states. The presence of the electron-deficient benzothiadiazole core, combined with chiral BINOL units, likely promotes enhanced spin–orbit coupling, stabilizing the triplet excitons and enabling long-lived emission.

Conclusions

The successful Suzuki cross-coupling reaction of 4,7-dibromo-5,6-(*R*/*S*)-BINOL-*O*-2,1,3-benzothiadiazole under catalytic conditions using $Pd(OAc)_2$ and SPhos ligand with various aryl boronic acids is reported with excellent yields (up to 94%). A range of 4,7-diarylated-5,6-(*R*/*S*)-BINOL-*O*-2,1,3-benzothiadiazoles have been synthesized and photophysically characterized by UV, FL and CD spectrometry. Especially, the Stokes shift of these compounds ranges from 128 to 192 nm, and they exhibit strong bathochromic emission shifts. Investigation of the circularly polarized luminescent properties showed strong electronic circular dichroism. The bandgaps of these compounds can be tuned by the Suzuki reaction and range between 2.71 and 3.51 eV, as revealed by DFT calculations.

Author contributions

Trang T. T. Pham and Phuong T. H. Chu carried out the synthesis; Bach L. D. Hoang and Chau M. Vo investigated the photophysical properties; Duan V. Le took care the synthesis of starting materials, Hien Nguyen and Thanh-Tuân Bui conducted the data analysis; Gioi V. Nguyen and Phuong T. H. Chu performed DFT calculations; G. Pieters and N. Salov performed the CPL measurements; Tung T. Dang conceived and supervised the project.

Conflicts of interest

There are no conflicts to declare.

Data availability

The full data can be found in the supplementary information (SI). All the raw original data will be made available upon reasonable request. Supplementary information is available. See DOI: https://doi.org/10.1039/d5ra09454b.

Acknowledgements

This research was funded by the Ministry of Education and Training, Vietnam, under grant number B2024.BKA.03. Tung T. Dang gratefully acknowledges the support for analytical measurements and photophysical studies provided through the CY Advanced Studies Program. We thank the Polish high performance computing infrastructure PLGrid for DFT calculations.

Notes and references

1 R. Pummerer, E. Prell and A. Rieche, *Ber. Dtsch. Chem. Ges. A/B*, 1926, **59**, 2159–2161.
2 J. M. Brunel, *Chem. Rev.*, 2005, **105**, 857–898.
3 Y. Chen, S. Yekta and A. K. Yudin, *Chem. Rev.*, 2003, **103**, 3155–3212.
4 D. Tauchi, T. Koida, Y. Nojima, M. Hasegawa, Y. Mazaki, A. Inagaki, K.-i. Sugiura, Y. Nagaya, K. Tsubaki, T. Shiga, Y. Nagata and H. Nishikawa, *Chem. Commun.*, 2023, **59**, 4004–4007.
5 Y. Yu, Y. Hu, C. Ning, W. Shi, A. Yang, Y. Zhao, Z.-Y. Cao, Y. Xu and P. Du, *Angew. Chem., Int. Ed.*, 2024, **63**, e202407034.
6 C. Yuan, K. Eguchi and H. Murata, *Jpn. J. Appl. Phys.*, 2024, **63**, 02SP10.
7 E. M. da Silva, H. D. A. Vidal, M. A. P. Januário and A. G. Corrêa, *Molecules*, 2023, **28**, 12.
8 J. Gao, P. Wang, A. Shen, X. Yang, S. Cen and Z. Zhang, *ACS Catal.*, 2024, **14**, 5621–5629.
9 Z. Li, P. Chen, Z. Ni, L. Gao, Y. Zhao, R. Wang, C. Zhu, G. Wang and S. Li, *Nat. Commun.*, 2025, **16**, 735.

10 M. Krajnc and J. Niemeyer, *Beilstein J. Org. Chem.*, 2022, **18**, 508–523.
11 P. Siripanich, J. Zhang, M. Lessio and C. Hua, *Mater. Chem. Front.*, 2025, **9**, 2087–2098.
12 F. Li, Y. Wang, Y. Sheng, G. Wei, Y. Cheng and C. Zhu, *RSC Adv.*, 2015, **5**, 105851–105854.
13 E. M. Sánchez-Carnerero, F. Moreno, B. L. Maroto, A. R. Agarrabeitia, M. J. Ortiz, B. G. Vo, G. Muller and S. de la Moya, *J. Am. Chem. Soc.*, 2014, **136**, 3346–3349.
14 C. Maeda, K. Nagahata, T. Shirakawa and T. Ema, *Angew. Chem., Int. Ed.*, 2020, **59**, 7813–7817.
15 S. Feuillastre, M. Pauton, L. Gao, A. Desmarchelier, A. J. Riives, D. Prim, D. Tondelier, B. Geffroy, G. Muller, G. Clavier and G. Pieters, *J. Am. Chem. Soc.*, 2016, **138**, 3990–3993.
16 S. Sun, J. Wang, L. Chen, R. Chen, J. Jin, C. Chen, S. Chen, G. Xie, C. Zheng and W. Huang, *J. Mater. Chem. C*, 2019, **7**, 14511–14516.
17 Y. Wang, Y. Zhang, W. Hu, Y. Quan, Y. Li and Y. Cheng, *ACS Appl. Mater. Interfaces*, 2019, **11**, 26165–26173.
18 L. Pu, *Chem. Rev.*, 2024, **124**, 6643–6689.
19 M. Coehlo, L. Frédéric, L. Poulard, N. Ferdi, L. Estaque, A. Desmarchelier, G. Clavier, J.-P. Dognon, L. Favereau, M. Giorgi, J.-V. Naubron and G. Pieters, *Angew. Chem., Int. Ed.*, 2025, **64**, e202414490.
20 L. Frédéric, A. Desmarchelier, L. Favereau and G. Pieters, *Adv. Funct. Mater.*, 2021, **31**, 2010281.
21 P. Kafourou, B. Park, J. Luke, L. Tan, J. Panidi, F. Glöcklhofer, J. Kim, T. D. Anthopoulos, J.-S. Kim, K. Lee, S. Kwon and M. Heeney, *Angew. Chem., Int. Ed.*, 2021, **60**, 5970–5977.
22 B. Amna, R. Isci, H. M. Siddiqi, L. A. Majewski, S. Faraji and T. Ozturk, *J. Mater. Chem. C*, 2022, **10**, 8254–8265.
23 S. Das, Y. Rout, M. Poddar, A. Z. Alsaleh, R. Misra and F. D'Souza, *Chem.–Eur. J.*, 2024, **30**, e202401959.
24 C. Wang, D. Xia, F. Yang, J. Li, Y. Wu and W. Li, *ACS Appl. Polym. Mater.*, 2021, **3**, 4645–4650.
25 L.-A. Lozano-Hernández, J. Cameron, C. J. Riggs, S. Reineke and P. J. Skabara, *ChemPhotoChem*, 2023, **7**, e202200256.
26 G. G. Dias, F. T. Souto and V. G. Machado, *Chemosensors*, 2024, **12**, 156.
27 C. P. Ebersol, N. P. Debia, H. C. Zimba, E. S. Moraes, D. S. Lüdtke, F. S. Rodembusch and A. V. Moro, *New J. Chem.*, 2024, **48**, 4680–4689.
28 M. Godfroy, J. Liotier, V. M. Mwalukuku, D. Joly, Q. Huaulmé, L. Cabau, C. Aumaitre, Y. Kervella, S. Narbey, F. Oswald, E. Palomares, C. A. González Flores, G. Oskam and R. Demadrille, *Sustainable Energy Fuels*, 2021, **5**, 144–153.
29 D. Gudeika, A. Miasojedovas, O. Bezvikonnyi, D. Volyniuk, A. Gruodis, S. Jursenas and J. V. Grazulevicius, *Dyes Pigm.*, 2019, **166**, 217–225.
30 F.-C. Kong, S.-Y. Yang, X.-J. Liao, Z.-Q. Feng, W.-S. Shen, Z.-Q. Jiang, D.-Y. Zhou, Y.-X. Zheng and L.-S. Liao, *Adv. Funct. Mater.*, 2022, **32**, 2201512.
31 D. Liu, W.-J. Wang, P. Alam, Z. Yang, K. Wu, L. Zhu, Y. Xiong, S. Chang, Y. Liu, B. Wu, Q. Wu, Z. Qiu, Z. Zhao and B. Z. Tang, *Nat. Photonics*, 2024, **18**, 1276–1284.